Contents lists available at SciVerse ScienceDirect

Computers & Geosciences

journal homepage: www.elsevier.com/locate/cageo

Quantifying multi-element and volumetric uncertainty, Coleman McCreedy deposit, Ontario, Canada

Ryan Goodfellow [a,*], Francisco Albor Consuegra [a], Roussos Dimitrakopoulos [a], Tim Lloyd [b]

[a] COSMO - Stochastic Mine Planning Laboratory, Department of Mining and Materials Engineering, McGill University, FDA Building, 3450 University Street, Montreal, Quebec, Canada H3A 2A7
[b] Vale, General Engineering Building, Hwy. 17 W, Door #10, Copper Cliff, Ontario, Canada P0M 1N0

ARTICLE INFO

ABSTRACT

Traditional geostatistical modelling of orebodies and estimation of grade–tonnage curves do not account for the uncertainty of the orebody grades and tonnages. Geological interpretations of complex shapes are often over-constrained, and therefore do not properly identify the location of the ore. In these situations, tonnage is often under-estimated and grade is over-estimated, resulting in orebody models used for mine planning that lead to costly financial decisions. This paper presents an approach aiming to better assess the uncertainty in an orebody model. The approach is applied to Vale's West Orebody of the Coleman McCreedy Mine, a poly-metallic deposit containing nickel, copper, gold, platinum and palladium. To encapsulate the orebody's variability and uncertainty, the nickel–copper sulphide mineralized zone is simulated using the single normal equation simulation method. The realizations serve as the orebody models from which the grades of multiple elements are jointly simulated using Min/Max Autocorrelation Factors. The final result is a series of equiprobable representations of the mineralization that incorporates both grade and tonnage uncertainty. The case study indicates that had conventional orebody estimations been used, there would have been a 10% over-estimation of orebody volume, along with significant over-estimation of low-grade material and under-estimation of high-grade material.

1. Introduction

In cases where drillhole spacing is particularly tight and the geological domains are continuous, deterministic mapping of geological domain boundaries (i.e. a wireframe) is likely to be sufficient in describing the mineralized volume of a deposit (Srivastava, 2005). To the contrary, deposits containing a mixture of two or more grade populations and uncertainty in the inter-pretation of the edges of the geological domains lead to substantial volumetric uncertainty, and stochastic treatment of the wireframes offers a suitable alternative (Osterholt and Dimitrakopoulos, 2007). Curvilinear geometries, typical in mineral deposits, are not prop-erly modelled using traditional two-point spatial statistics such as variograms (Journel, 2007). The reproduction of geometries calls for the consideration of the joint categorical variability at three or more points at a time. Strebelle (2002) proposed a stochastic simulation algorithm that does not require variogram modelling

and is based on extracting the so-called multiple point (MP) statistics from a training image (Strebelle, 2002). Some recent developments on multiple-point methods include a list-based storage of patterns (Straubhaar et al., 2011), directly sampling patterns from the training image (Mariethoz et al., 2010), filter and pattern-based simulations (Zhang et al., 2006; Arpat and Caers, 2007) and high-order simulation (Mustapha and Dimitrakopoulos, 2010).

Geological deposits typically contain several variables of interest that are spatially correlated. The use of joint geostatistical techni-ques that maintain spatial correlation are not new (David, 1988; Goovaerts, 1997), however, the computational costs associated with the simulation increase significantly with more variables, and require modelling of cross-correlations, which substantially increases with the number of variables being jointly simulated. A practical alternative to the 'direct' joint-simulation of variables is the decorrelation of variables introduced using principal compo-nent analysis or PCA (David, 1988; Wackernagel, 2003). The effectiveness of this approach is limited because PCA does not eliminate cross-correlations at distances other than zero. To over-come the limitations associated with PCA, minimum/maximum autocorrelation factors, MAF (Desbarats and Dimitrakopoulos, 2000; Boucher and Dimitrakopoulos, 2009; Dimitrakopoulos and

---

* Corresponding author. Tel.: +1 514 398 4755x094748; fax: +1 514 398 7099.
E-mail addresses: ryan.goodfellow@mail.mcgill.ca (R. Goodfellow),
francisco.alborconsuegra@mail.mcgill.ca (F. Albor Consuegra),
roussos.dimitrakopoulos@mcgill.ca (R. Dimitrakopoulos),
tim.lloyd@vale.com (T. Lloyd).

Fonseca, 2003; Lopes et al., 2011) may be used to decorrelate pertinent variables into spatially non-correlated factors that are independently simulated and back transformed to correlated attributes. To further reduce the time required to simulate the deposit for the variables of interest, MAF can readily be integrated with the direct block simulation method (Boucher and Dimitrakopoulos, 2009).

In the following sections, a general overview of multiple-point simulation is given, followed by an overview of joint simulation of multiple correlated variables using Min/Max Autocorrelation Factors at the block support scale. Both methods are then applied to a case study at Vale's West Orebody at the Coleman McCreedy deposit, by first simulating the ore envelope and subsequently simulating the grades for gold, copper, nickel, palladium and platinum jointly within the models. Following this, the results from the generated grade–volume curves are discussed in terms of volumetric uncertainty and grade variability within the generated models. Finally, conclusions from this case study are presented.

2. Multiple-point simulation of orebody models

2.1. Definitions

Multiple-point statistics, or MP-statistics, consider a neighbourhood of any n number of surrounding points jointly. The geometric configuration of a multiple-point data event d_n centred at node A is called a template, τ_n, of size n. The size of the template, n, and its shape can be configured to capture any data events that inform the central node A. Fig. 1 shows an example of a data event on a template with $n=4$ (Osterholt and Dimitrakopoulos, 2007).

Specifically, consider an attribute S taking K possible categorical states $\{s_k, k=1,\ldots,K\}$, which may represent, for example, lithological codes or metallurgical ore types. A geometric template τ_n is defined by a set of n vectors $\{\mathbf{h}_\alpha, \alpha=1,\ldots,n\}$. A data event d_n of size n, centred at the location or node $\mathbf{x}$, is defined by the vectors in the template τ_n, offset from a central location $\mathbf{x}$. The data event consists of a set of measured categorical state values $s(\mathbf{x}+\mathbf{h}_\alpha)$ at locations $(\mathbf{x}+\mathbf{h}_\alpha), \alpha=1,\ldots,n$. Any permutation of data values $s(\mathbf{x}+\mathbf{h}_\alpha), \alpha=1,\ldots,n$ for the set of vectors $\{\mathbf{x}+\mathbf{h}_\alpha, \alpha=1,\ldots,n\}$ represents a distinct data event, hence will represent a different MP-statistic.

Given that MP statistics are often used to characterize spatial relationships of closely spaced data, training images (TIs) are used to supplement the multiple-point statistics that cannot be inferred from sparse drilling data alone. The geometries and underlying patterns contained in a training image should be consistent with the geological concept and interpretation of the deposit.

2.2. A conditional simulation algorithm for MP-geostatistics

Whereas traditional variogram-based conditional simulation methods estimate a conditional distribution function by solving
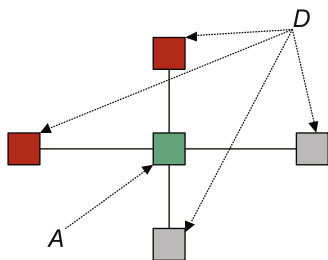

Fig. 1. Example of a data template. The central node A is to be simulated using the n surrounding known data events, D.

a kriging system consisting of two-point covariances, the MP conditional distribution is conditioned to a single joint MP data event d_n:

$$f(\mathbf{x}; s_k|d_n) = E\{I(\mathbf{x}; s_k)|d_n\} = Pr\{S(\mathbf{x}) = s_k|d_n\}, \quad k=1,\ldots,K \quad (1)$$

where $f(\mathbf{x}; s_k|d_n)$ is the conditional probability that $s(\mathbf{x}) = s_k$ given the data event d_n and $E\{I(\mathbf{x}; s_k)|d_n\}$ is the conditional expectation of the indicator function $I(\mathbf{x}; s_k)$ given the data event d_n, whereby $I(\mathbf{x}; s_k) = 1$ if $s(\mathbf{x}) = s_k$, otherwise $I(\mathbf{x}; s_k) = 0$.

Let A_k denote the binary random variable indicating the occurrence of data event d_n at location $\mathbf{x}$

$$A_k = \begin{cases} 1 & \text{if } S(\mathbf{x}) = s_k \\ 0 & \text{otherwise} \end{cases} \quad (2)$$

Similarly, let D denote a binary random variable indicating the occurrence of data event d_n. The conditional probability of the node or location $\mathbf{x}$ corresponding to state s_k is given by the following simple indicator kriging expression:

$$f(\mathbf{x}; s_k|d_n) = Pr\{A_k = 1|D = 1\} = E\{A_k\} + \lambda[1 - E\{D\}] \quad (3)$$

where $E\{D\} = Pr\{D = 1\}$ is the probability of the conditioning data event d_n occurring and $E\{A_k\} = Pr\{S(\mathbf{x}) = s_k\}$ is the prior probability for the state at location $\mathbf{x}$ is s_k. Solving the simple kriging system for the single weight λ corresponding to data event d_n leads to the following solution (Guardiano and Srivastava, 1993):

$$f(\mathbf{x}; s_k|d_n) = Pr\{A_k = 1|D = 1\} = \frac{Pr\{A_k = 1, D = 1\}}{Pr\{D = 1\}} \quad (4)$$

The numerator and denominator of Eq. (4) are inferred by scanning the training image for both the number of replicates of the conditioning data event $c(d_n)$, and the number of replicates $c_k(d_n)$ from the set of replicates $c(d_n)$ that have $S(\mathbf{x}) = s_k$, i.e.

$$f(\mathbf{x}; s_k|d_n) = \frac{c_k(d_n)}{c(d_n)} \quad (5)$$

In the SNESIM (single normal equation simulation) algorithm (Strebelle, 2002), the available conditioning data forming the data event d_n is stored in a search tree. The proportions for building the ccdf are retrieved by searching for similar data events in the search tree reading the related frequencies. In MP geostatistics, there is no need to approximate the use of the global conditioning data event due to the use of a training image and the exact calculation of the probability distribution conditional to d_n. It must be noted that given that all MP statistics are derived from the patterns present in the training image, the algorithm is said to be "training-image driven"; the conditioning samples represented by, for example, drillhole data merely guide the algorithm to search for patterns from the training image that fit the same data configuration d_n. For this reason, it must be assumed that the training image is an accurate representation of reality. For a more detailed discussion on the SNESIM algorithm, the reader is referred to Remy et al. (2011). An overview of the general steps of the simulation is given below:

1. Scan the training image and store occurrences of all data events D.
2. Define a random path and visit all nodes to be simulated.
3. Simulate each node by:
   a. Retrieving all data events containing the surrounding data and previously simulated nodes.
   b. Derive the local probability distribution from stored frequencies of central values; the probability of finding a certain categorical variable at the node given the surrounding data event D is given by the Bayes' relation for conditional probability in Eq. (5).
   c. Randomly select a pattern from the distribution and add simulated node to the grid.
4. Repeat the previous steps for a desired number of simulations.

3. Joint simulation of correlated variables with Minimum/Maximum Autocorrelation Factors

Consider a multivariate, stationary and ergodic spatial random function of a continuous variable $\mathbf{Z}(\mathbf{x}) = [Z_1(\mathbf{x}, \ldots, Z_p(\mathbf{x})]^T$ that has been transformed to a standard Gaussian random function $\mathbf{Y}(\mathbf{x}) = [Y_1(\mathbf{x}, \ldots, Y_p(\mathbf{x})]^T = [\phi(Z_1(\mathbf{x})), \ldots, \phi(Z_p(\mathbf{x}))]^T$ and is assumed to be multi-Gaussian. Minimum/Maximum Autocorrelation Factors (MAFs) are defined as the p orthogonal linear combinations $M_i(\mathbf{x}) = a_i^T \mathbf{Y}(\mathbf{x}), i = 1, \ldots, p$ of the original multivariate vector $\mathbf{Y}(\mathbf{x})$. MAFs are derived assuming that $\mathbf{Y}(\mathbf{x})$ is represented by a two-structure linear model of coregionalization (Desbarats and Dimitrakopoulos, 2000). The MAF transformation can be rewritten as

$$\mathbf{M}(\mathbf{x}) = \mathbf{A}_{MAF}^T \mathbf{Y}(\mathbf{x}) = \mathbf{A}_{MAF}^T \phi(\mathbf{Z}(\mathbf{x})) \tag{6}$$

and the MAF factors, $\mathbf{A}_{MAF}$, are derived from

$$\mathbf{A}_{MAF} = \mathbf{Q}_2 \Lambda_1^{-1} \mathbf{Q}_1 \tag{7}$$

where the eigenvectors $\mathbf{Q}_1$ and eigenvalues Λ_1 are obtained from the spectral decomposition of the multivariate covariance matrix $\mathbf{B}$ of $\mathbf{Y}(\mathbf{x})$ at the zero-lag distance. More specifically, the spectral decomposition is computed as

$$\mathbf{Q}_1 \mathbf{B} \mathbf{Q}_1^T = \Lambda_1 \tag{8}$$

$\mathbf{Q}_2$ is the matrix of eigenvectors from the following spectral decomposition:

$$\mathbf{Q}_2(\tfrac{1}{2}[\Gamma_\zeta(\Delta)]^T + [\Gamma_\zeta(\Delta)])\mathbf{Q}_2^T = \Lambda_2 \tag{9}$$

where the matrix $\Gamma_\zeta(\Delta)$ is an asymmetric variogram matrix at lag distance Δ for the regular PCA factors $\zeta(\mathbf{x}) = \mathbf{Y}(\mathbf{x})\mathbf{A}$, where $\mathbf{A} = \mathbf{Q}_1 \Lambda_1^{-1/2}$. Λ_2 is the matrix of eigenvalues obtained from the spectral decomposition in Eq. (9). In practice, the simplest way to ensure that the transformed variables are orthogonal is to test the cross-variograms of the MAF factors for several lag distances, Δ, and select the one which provides the best decorrelation; this method permits applying the MAF transformation to the experimental data set without having to derive theoretical variogram and cross-variogram models beforehand. For a more detailed description of MAF for simulation of correlated attributes, the reader is referred to Desbarats and Dimitrakopoulos (2000).

The direct block simulation method (Godoy, 2003), and more specifically direct block simulation for multiple correlated variables (Boucher and Dimitrakopoulos, 2009), is used to simulate the MAF factors $\mathbf{M}(\mathbf{x})$ independently for each of the blocks in the domain $D \in \Re^n$. Simulation at the block-support scale using MAF calls for the block support vector random function $\mathbf{Z}_V$, which can be expressed as

$$\mathbf{Z}_V(\nu) = \frac{1}{N} \sum_{i=1}^{N} \phi^{-1}((\mathbf{A}_{MAF}^T)^{-1}\mathbf{M}(\mathbf{x}_i)), \quad \mathbf{x}_i \in \nu, \quad \forall i \tag{10}$$

where each block $\nu \in D$ is discretized by N points at locations $\mathbf{x}_i \in \nu$ and $\{i = 1, \ldots, N\}$ denotes the indices for each of the discretization points. For each block to be simulated, the discretizing point values conditional to neighbouring point and block data are simulated with the joint LU simulation. Let $\mathbf{C}_{IIVV}^l$ be the covariance matrix for the conditioning data and $\mathbf{C}_{IV}^l$ be the covariance matrix between the simulation grid's points and the neighbouring point and block data for the lth MAF factor

$$\mathbf{C}_{IIVV}^l = \begin{bmatrix} \mathbf{C}_{II}^l & \mathbf{C}_{IV}^l \\ \mathbf{C}_{VI}^l & \mathbf{C}_{VV}^l \end{bmatrix} \quad \text{and} \quad \mathbf{C}_{pIV}^l = \begin{bmatrix} \mathbf{C}_{pI}^l & \mathbf{C}_{pV}^l \end{bmatrix} \tag{11}$$

where $\mathbf{C}_{II}^l$, $\mathbf{C}_{IV}^l$ and $\mathbf{C}_{VV}^l$ are the point-to-point, point-to-block and block-to-block covariance matrices for the lth MAF factor, respectively; $\mathbf{C}_{pI}^l$ and $\mathbf{C}_{pV}^l$ define the covariances between the discretizing

points and the point data and the block data for the lth MAF factor, respectively. The vector of N simulated values $\mathbf{m}_p^{l*}$ for each factor l is obtained by solving the following system of equations similar to generating LU simulations with conditioning data (Godoy, 2003; Boucher and Dimitrakopoulos, 2009)

$$\mathbf{m}_p^{l*} = \mathbf{L}_{pIV}^l (\mathbf{L}_{IIVV}^l)^{-1}\mathbf{m}_{IV}^l + \mathbf{L}_{pp}^l \mathbf{w}_p \tag{12}$$

where $\mathbf{m}_{IV}^l$ is the vector containing neighbouring point and block data for factor l, $\mathbf{w}_p$ is a vector of randomly generated standard normal numbers and $\mathbf{L}_{pIV}^l$, $\mathbf{L}_{IIVV}^l$ and $\mathbf{L}_{pp}^l$ are obtained from the following Cholesky decomposition:

$$\begin{bmatrix} \mathbf{C}_{IIVV}^l & \mathbf{C}_{pIV}^l \\ \mathbf{C}_{pIV}^l & \mathbf{C}_{pp}^l \end{bmatrix} = \begin{bmatrix} \mathbf{L}_{IIVV}^l & 0 \\ \mathbf{L}_{pIV}^l & \mathbf{L}_{pp}^l \end{bmatrix} \begin{bmatrix} \mathbf{L}_{IIVV}^{l^T} & \mathbf{L}_{pIV}^{l^T} \\ 0 & \mathbf{L}_{pp}^{l^T} \end{bmatrix} \tag{13}$$

The block value can be obtained by averaging the back-transformed points that discretize each block with Eq. (12). The direct block MAF simulation algorithm (Boucher and Dimitrakopoulos, 2009) proceeds as follows:

1. Transform the data $\mathbf{Z}(\mathbf{x})$ to normal-score data $\mathbf{Y}(\mathbf{x})$.
2. Transform $\mathbf{Y}(\mathbf{x})$ to $\mathbf{M}(\mathbf{x})$ using the MAF transformation in Eq. (6).
3. Define a random path to visit each block to be simulated.
4. For each block ν, simulate the MAF factors at each of the block's N discretizing points $\mathbf{m}^*(\mathbf{x}_i), i = 1, \ldots, N$ with the LU decomposition using Eq. (12).
   a. Average the points $\mathbf{m}^*(\mathbf{x}_i), i = 1, \ldots, N$ over the block to obtain $\mathbf{m}_V^*(\nu)$ for further conditioning.
   b. Back-transform the simulated nodes $\mathbf{m}^*(\mathbf{x}_i), i = 1, \ldots, N$ to $\mathbf{z}^*(\mathbf{x}_i)$ and average the points $\mathbf{x}_i \in \nu$ to obtain the simulated value at the block support scale, $\mathbf{z}_V^*(\nu)$ using Eq. (10). Write the values to a file.
5. Repeat step (4) for each block ν to be simulated.
6. Repeat steps (3)–(5) to generate a set of multi-element geological simulations.

4. Geology of the West Orebody

Vale's West Orebody (WOB), located in Sudbury, Ontario, Canada, is located 1463 m west of the Lower Coleman Orebody. It has a known strike length of 213 m. The ore thickness ranges from 1.5 to 46 m with an average of 27 m. The upper portion of the orebody dips steeply to the south at 80° before flattening to 40° at depth. The orebody is composed of massive sulphides, stringer sulphides, and weaker disseminations within granite breccia zones enclosed in the host footwall rocks. The host rocks are granite gneiss, granite breccia and Sudbury breccia.

5. Simulation of the ore envelope

5.1. TI and hard data

A conventional deterministic orebody model is used to serve as a training image for the simulation process. To generate the model, the drillhole data is coded as inside (1) or outside (0) the nickel–copper mineralized zone based on the presence low-grade nickel. A wireframe envelope is generated and converted to a block model on a regular grid, whereby all blocks that lie within the mineral envelope (wireframe) are designated as mineralized material (1) and all other blocks are designated as barren rock (0). It is noted that the low-grade nickel criterion, hence the wireframe envelope, is subject to interpretation; a single, smooth and connected orebody model is generally preferred by the geologist. The conventional model is used as a training image and is

comprised of $31 \times 84 \times 80$ blocks with dimensions of $6.1 \times 4.6 \times 4.6$ m^3. A cross-section of the training image is shown in Fig. 2(a). The hard data used for the simulations is obtained from 15,319 drillhole samples composited over 1.52-m lengths.

5.2. Orebody simulation, specifics and post-processing

To assess the geological uncertainty in terms of volume and tonnage, a set of 20 realizations of the orebody are generated using the SNESIM algorithm (Strebelle, 2002; Osterholt and Dimitrakopoulos, 2007). The simulations are generated on the same grid as the conventional model (training image) defined in Section 5.1. Since this is a single orebody, connectivity for the blocks is expected. In this application, the SNESIM algorithm found it difficult to retrieve sufficient information related to the connectivity and orientation of geological features in the orebody in order to guarantee realizations that consisted of a single completely connected orebody. One solution employed to overcome this issue was to increase the number of nodes in the template, thus providing more information to a node being simulated. This, however, raises the computational costs for the simulations.

Nevertheless, the connectivity issue was not completely overcome, and the realizations required post-processing to remove randomly allocated ore blocks in the model. A simulated annealing-based algorithm (Deutsch and Journel, 1998) is used to post-process the simulations to better-reproduce the two-point continuity of the training image. Osterholt and Dimitrakopoulos (2007) also document similar issues related to connectivity and smoothness when simulating iron ore channels. The "cleaned" realizations are referred simply as realizations in the subsequent sections.

5.3. Validation

Fig. 2 shows how the simulated realizations reproduce the large-scale features of the training image, such as the steeply dipping of the upper portion of the orebody and its flattening with depth. The algorithm (Remy et al., 2011) allows the realizations to reproduce the target waste proportion of 93.2%; the waste proportions of the 20 realizations fluctuate between 93.2% and 94.1% with a mean of 93.9%. Fig. 3 shows the indicator variogram reproduction for the SNESIM realizations, training image and data. The indicator variogram for vector $\mathbf{h}$, $\gamma_I(\mathbf{h}; s_k)$, is calculated using:

$$\gamma_I(\mathbf{h}; s_k) = \frac{1}{2N(\mathbf{h})} \sum_{\alpha=1}^{N(\mathbf{h})} [I(\mathbf{x}_\alpha; s_k) - I(\mathbf{x}_\alpha + \mathbf{h}; s_k)]^2 \qquad (14)$$

where $N(\mathbf{h})$ denotes the number of pairs of points separated by the vector $\mathbf{h}$, and the α is used to index these pairs. It is first noted that the simulations accurately reproduce the indicator variogram of the training image, however the variability for both the simulations
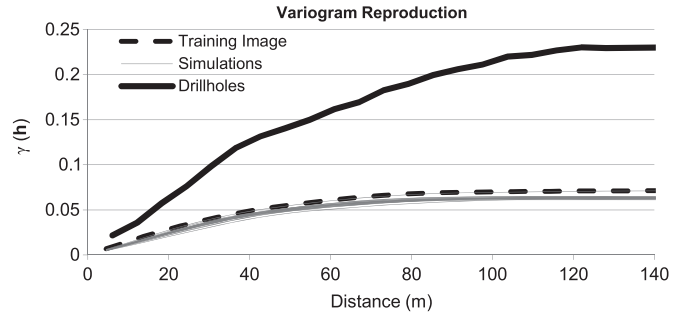
Fig. 3. Indicator variogram reproduction of the post-processed simulations.
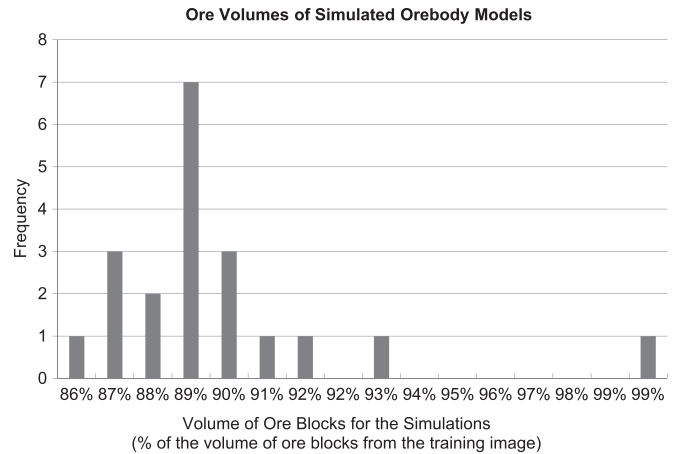
Fig. 4. Frequency distribution of the volume of ore for the post-processed SNESIM realization as a percentage of the volume of ore blocks in the training image.

and training image are significantly less than the variability in the data. This behaviour is to be expected, given that the algorithm is driven by the patterns available in the training image rather than a variogram model; additionally, the post-processing step enhances the training image's variogram reproduction. The significant difference between indicator variograms suggests that there is a conflict between the data and the training image, and is a result of choosing a single, smooth and connected orebody model rather than using a model that strictly obeys the low-grade nickel coding applied to the drillholes. These issues have also been studied by Osterholt and Dimitrakopoulos (2007) when simulating an iron ore channel. To deal with such cases where there is a conflict between the data and training image, data-driven methods, such as high-order simulation with spatial cumulants (Mustapha and Dimitrakopoulos, 2010; Dimitrakopoulos et al., 2010), need to be explored.

5.4. Assessing volumetric uncertainty

To assess the grade–tonnage uncertainty present in the modelling of the deposit, the realizations generated by SNESIM are used as distinct orebody models from which nickel, copper, gold, palladium and platinum are jointly simulated. The frequency distribution, in terms of the percentage total volume of ore in the simulation compared to the volume of ore in the training image, is shown in Fig. 4. It is noted that the volume of the ore blocks of the training image (a conventional deterministic wireframe generated by a geologist) is approximately 10% higher than the volume of the simulations. This highlights the need for the generation of multiple objective orebody models when assessing a mineral deposit. For the purpose of this study, the simulated models with the maximum, median and minimum ore

Fig. 2. Example of a data template. Cross-sections of (a) the training image, (b) cleaned maximum, (c) cleaned median and (d) cleaned minimum simulated models of the deposit (in terms of volume).

volumes are retained for further joint multi-element simulation, and are referred to as the Max, Med and Min orebody models. It is noted that in general, all simulations should be retained for joint multi-element simulation. However, in this case there is very little difference in terms of volumetrics for the majority of the simulations (with the exception of the Max orebody model), which is a result of the high drilling density within the miner-alized zone. Fig. 2 shows sample cross-sections of the selected orebody models.

6. Joint simulation of nickel, copper, gold, palladium and platinum

6.1. Normal score and MAF transformation

Similar to traditional orebody estimation methods, the drill-holes are filtered for each orebody model, such that only the drillholes inside the model are kept. Prior to applying the MAF transformations to the spatially correlated variables, each of the elements is transformed to a normal distribution. Normal score transformations are based on rank ordering of the data and decrease the influence of outliers. The transformation matrix $\mathbf{A}_{MAF}$ (Eq. (7)) for the median orebody is shown in Table 1. MAF are calculated by multiplying the vector of Cu, Ni, Au, Pd and Pt by a vector of loadings from the rows of the transformation matrix. The Δ lag in Eq. (9) used in this example is 9 m, and is derived experimentally by testing several lag distances to assure a suitable decorrelation and stable MAF decomposition.

6.2. Variography of MAF

The variogram models used for simulating each of the MAF factors in the median orebody model are presented in Table 2. Each of the variogram models was assumed to contain a nugget and a spherical structure. It is noted that MAF variograms are linear combinations of the variograms of the original (normal score) variables; the variogram models of the MAF factors does not necessarily correspond to the variography of the variables.

6.3. Conditional simulation of MAF at the block support scale

Conditional simulations for each of the factors in each of the orebody models are performed independently using Eq. (12) and averaged into blocks using Eq. (10); the point support informa-tion is retained for a variogram validation with the drillholes. The simulations are generated inside the orebody models using $6.1 \times 4.6 \times 4.6$ m^3 blocks and a $4 \times 3 \times 3$ node discretization density on the same grid as the wireframe, resulting in 502,524, 446,940 and 436,536 nodes within the limits of the maximum, median and minimum simulated orebody models, respectively. Ten simulations for each of the factors are generated for each of the three simulated orebody models and are validated in detail for reproduction of data, histograms and variograms on the point support. Fig. 5 shows a cross-variogram between the first two MAF factors for the median model. As one would expect during simulation, there are no spatial cross-correlations between the two factors, hence the MAF factors are indeed independent and have been successfully decorrelated. The remaining cross-variograms are very similar to the one presented, thus are omitted. A validation of variograms, cross-variograms and histograms is presented only for the data space in the subsequent section.

6.4. Validation of results

Validation of the jointly simulated variables involves calcula-tion of histograms, experimental variograms and cross-vario-grams of the simulated point realizations in the data space to ensure reproduction of original data and their spatial character-istics. Fig. 6 shows the variograms and cross-variograms for the original drillhole data and conditional simulations for the median orebody at the point support scale. All results suggest that the reproduction of the original data spatial characteristics by the simulated realizations is reasonable. Recall that the variograms and cross-variograms of original variables are not directly used in the joint simulation based on MAF, which used the variograms of the independent MAF. Fig. 7 shows the reproduction of the histograms of the 10 simulations and the original drillhole data for Au, Cu, Ni, Pd and Pt in the median orebody. All graphs indicate that the simulations reproduce well the initial drillhole data. Fig. 8 shows sample cross-sections for each of the simulated metals inside the Min, Med and Max orebody models. It is noted that by inspection, the grades are similar in all of the models, however there are some fairly significant differences in the shapes of the models, which highlights the benefits of generating a series of equiprobable orebody models to obtain a better understanding of volumetric variations.
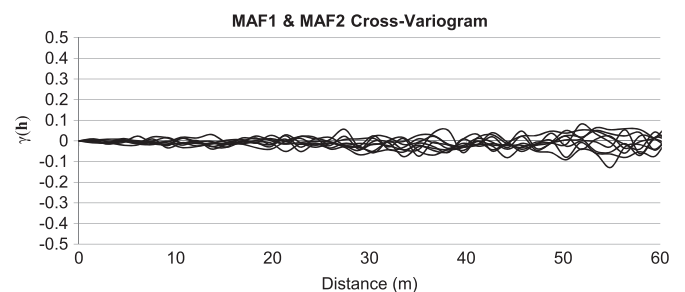
Table 1
MAF factor loadings described as linear combinations of the input variables for the median (Med) orebody model.

Metal	MAF 1	MAF 2	MAF 3	MAF 4	MAF 5
Au	0.063	−0.292	0.181	−0.009	−0.054
Cu	0.783	0.210	0.012	0.240	0.154
Ni	0.296	0.015	0.038	0.168	0.391
Pd	0.539	0.917	0.940	0.731	0.762
Pt	−0.070	0.173	0.287	0.617	0.490

Table 2
Variogram models used to simulate the MAF factors for the median (Med) orebody.

Variable	Variogram model	Major (x)		Minor (z)	
		AZ°	DIP°	AZ°	DIP°
MAF 1	$\gamma(\mathbf{h}) = 0.54 + 0.46 sph\left(\frac{h_x}{19}, \frac{h_y}{15}, \frac{h_z}{6}\right)$	90	0	0	90
MAF 2	$\gamma(\mathbf{h}) = 0.48 + 0.52 sph\left(\frac{h_x}{43}, \frac{h_y}{30}, \frac{h_z}{17}\right)$	135	0	45	168
MAF 3	$\gamma(\mathbf{h}) = 0.56 + 0.44 sph\left(\frac{h_x}{37}, \frac{h_y}{26}, \frac{h_z}{10}\right)$	135	0	45	68
MAF 4	$\gamma(\mathbf{h}) = 0.41 + 0.59 sph\left(\frac{h_x}{44}, \frac{h_y}{44}, \frac{h_z}{44}\right)$	135	0	45	−45
MAF 5	$\gamma(\mathbf{h}) = 0.41 + 0.59 sph\left(\frac{h_x}{51}, \frac{h_y}{40}, \frac{h_z}{17}\right)$	225	45	225	−45

Fig. 5. Example of a cross-variogram between MAF 1 and MAF 2 for all simula-tions from the median orebody.
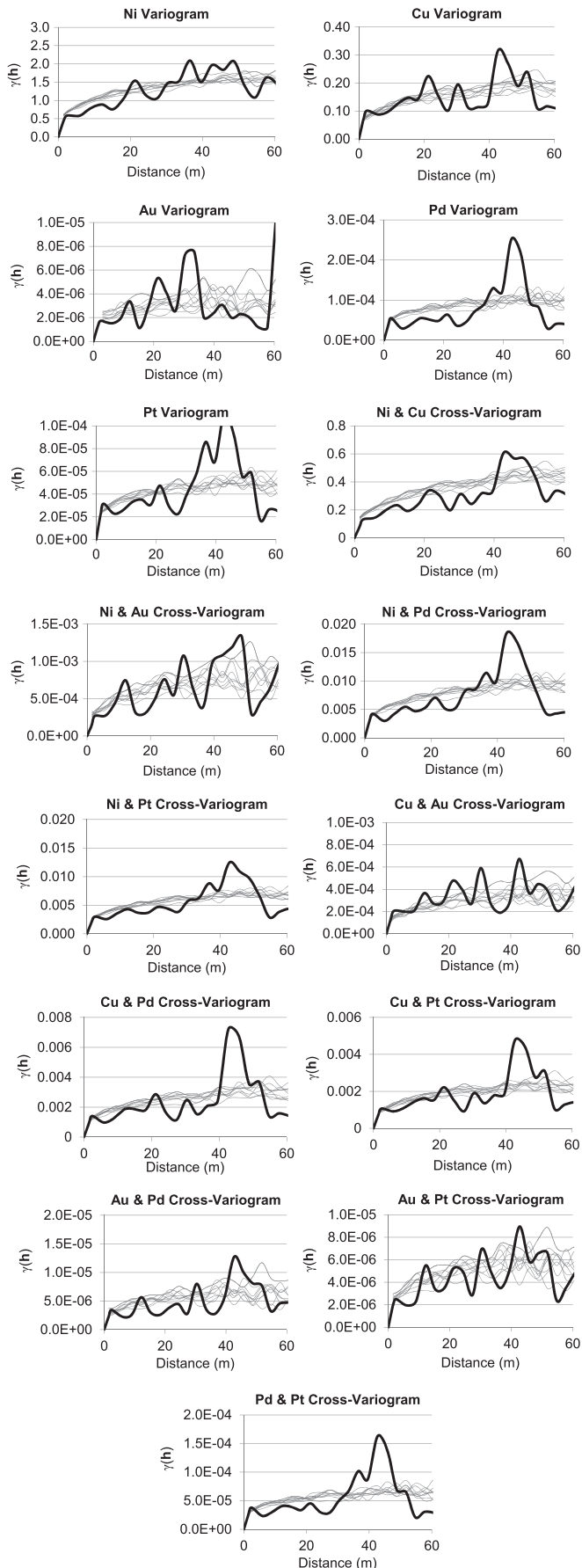
Fig. 6. East–West variogram and cross-variogram reproduction for the median orebody (note that the heavy line is the drillhole variogram and the light lines are simulations).
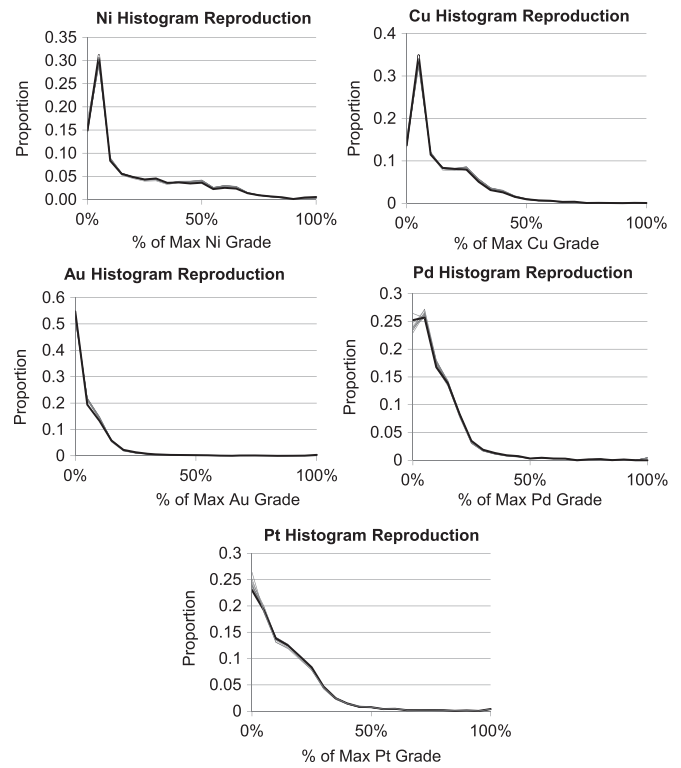

Fig. 7. Histogram reproduction of the 10 simulations and original drillholes for Ni, Cu, Au, Pd and Pt in the median orebody model.

7. Risk analysis for decision making

To better understand the relationship between volumes and grades for the deposit, Fig. 9 shows the changes in volume for a nickel cutoff grade for the $6.1 \times 4.6 \times 4.6$ m^3 blocks. It is noted that in the graph, the volumes above a cutoff for the Min and Med orebodies are very close, and it is difficult to distinguish between the sets of simulations. The volumes above a certain cutoff grade are significantly higher for the Max orebody simulations, which is to be expected given that the Max model has a 10% larger volume than the Med model (whereas the Min model is only 2% smaller than the Med model). This trend is particularly apparent for low cutoff grades for all of the metals; at higher cutoffs, all of the curves for the Min, Med and Max orebodies converge.

As a basis for comparison, the nickel grade is estimated within the training image using ordinary kriging. The volume–cutoff curve for this model (Fig. 9) highlights the importance of incorporating both volumetric and grade uncertainty into the geology models. It is clear that in this case study (however not necessarily in general), neglecting to incorporate the volumetric uncertainty would lead to a significant over-estimation of the orebody volume, as can be seen at low cutoffs in Fig. 9. This figure also highlights the importance of stochastic simulation methods over conventional grade estimation methods, which would have led to a model that overestimates the low-grade material and underestimates the high-grade material. It is clear that using the traditional geostatistical methods, comprised of creating a subjective and deterministic orebody model and estimating within that model may lead to costly business decisions in the mine planning phase.

8. Conclusions

This paper presents an approach to assess volumetric and multiple-element uncertainty, and is applied at West Orebody of Vale's
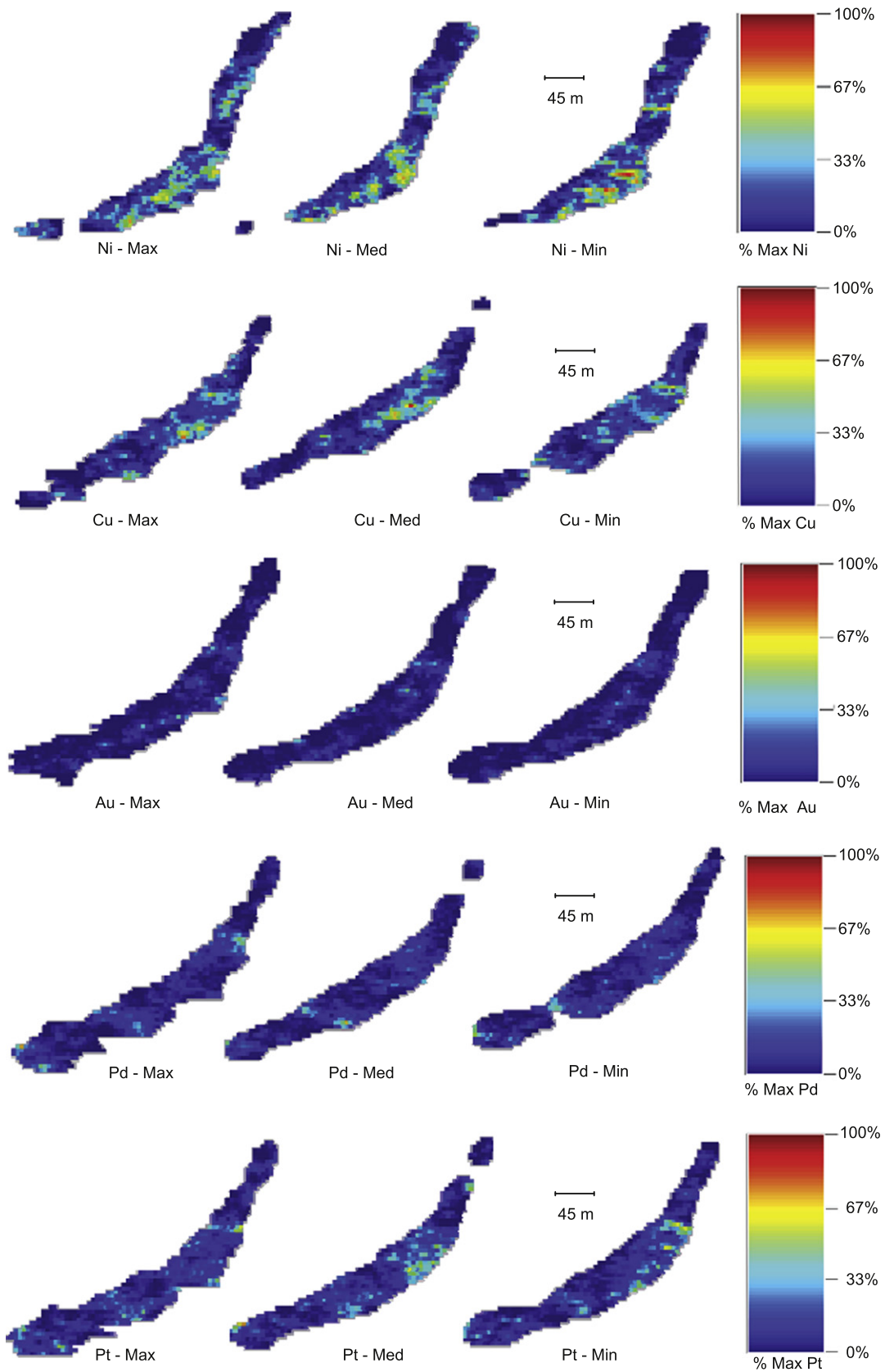
Fig. 8. Volume above Ni cutoff grade curves for the simulated orebodies with $6.1 \times 4.6 \times 4.6$ m^3 blocks.

Coleman McCreedy deposit, located in Sudbury, Ontario, Canada. In order to better quantify the spatial relationships, curvilinear features and volumetric uncertainty in the orebody, SNESIM, a multiple-point geostatistics method, was first used to simulate a series of equiprobable orebody models. A conventional, deterministic orebody model is used as a training image to provide a set of patterns for the simulation
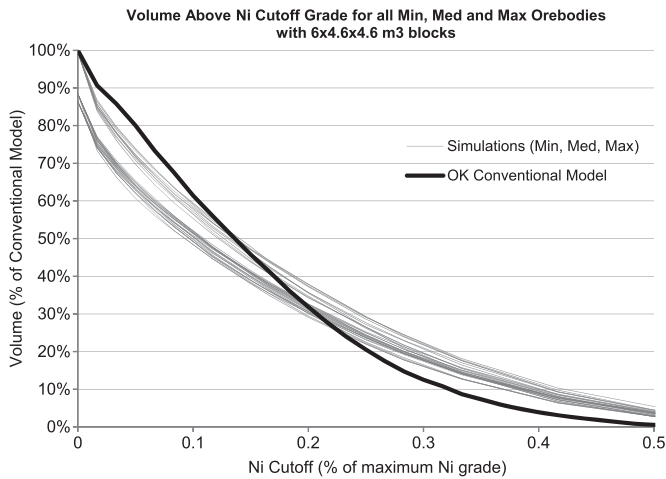
Fig. 9. Volume above Ni cutoff grade curves for the simulated orebodies with $6.1 \times 4.6 \times 4.6$ m^3 blocks.

algorithm. Given that there is a conflict between the data and the training image in terms of spatial correlations and proportions, the majority of the simulated orebody models require post-processing to enforce the geologists' connectivity requirement in the orebody. A subset of the simulations, specifically the orebody models that represent the highest, intermediate and minimum quantities of mineralized material, are then retained for joint simulation of nickel, copper, gold, platinum and palladium using Min/Max Autocorrelation Factors and Direct Block Simulation. This method permits the efficient joint simulation of the spatially correlated metals without having to fit cross-variogram models for each pair of elements. The result is a set of equiprobable orebody models that account for both volumetric and multi-metal uncertainty. Results indicate that had a conventional, deterministic orebody model been used with conventional grade estimation methods, there could have been as much as 10% over-estimation of low-grade mineralized material. In order to alleviate the issues with conflicts between training images and data, future work will focus on data-driven high-order stochastic simulation methods for simulating indicator variables (orebody models) and joint simulation for multiple elements.

References

Arpat, G.B., Caers, J., 2007. Conditional simulation with patterns. Mathematical Geosciences 39 (2), 177–203. doi:10.1007/s11004-006-9075-3.

Boucher, A., Dimitrakopoulos, R., 2009. Block simulation of multiple correlated variables. Mathematical Geosciences 41 (2), 215–237. doi:10.1007/s11004-008-9178-0.

David, M., 1988. Handbook of Applied Advanced Geostatistical Ore Reserve Estimation. Elsevier, Amsterdam 232 pp.

Desbarats, A.J., Dimitrakopoulos, R., 2000. Geostatistical simulation of regionalized pore-size distributions using Min/Max autocorrelation factors. Mathematical Geology 32 (8), 919–942. doi:10.1023/A:1007570402430.

Deutsch, C.V., Journel, A.G., 1998. GSLIB: Geostatistical Software Library: and User's Guide, 2nd ed. Oxford University Press, New York, NY 369 pp.

Dimitrakopoulos, R., Fonseca, M., 2003. Assessing risk in grade-tonnage curves in a complex copper deposit, northern Brazil, based on an efficient joint simulation of multiple correlated grades. In: Proceedings of the Application of Computers and Operations Research in the Minerals Industries, Cape Town, South Africa, pp. 373–382.

Dimitrakopoulos, R., Mustapha, H., Gloaguen, E., 2010. High-order statistics of spatial random fields: exploring spatial cumulants for modeling complex non-Gaussian and non-linear phenomena. Mathematical Geosciences 42 (1), 65–99. doi:10.1007/s11004-009-9258-9.

Godoy, M., 2003. The Effective Management of Geological Risk in Long-Term Scheduling of Open Pit Mines. Ph.D. Dissertation. University of Queensland, Brisbane, Australia, 256 pp.

Goovaerts, P., 1997. Geostatistics for Natural Resources Evaluation. Oxford University Press, New York, 496 pp.

Guardiano, F., Srivastava, M., 1993. Multivariate geostatistics: beyond bivariate moments. In: Geostatistics-Troia. Kluwer Academic, Amsterdam, pp. 133–144.

Journel, A.G., 2007. Roadblocks to the evaluation of ore reserves—the simulation overpass and putting more geology into numerical models of deposits. 2nd ed. In: Dimitrakopoulos, R. (Ed.), Orebody Modelling and Strategic Mine Planning, Spectrum Series, vol. 14. The Australasian Institute of Mining and Metallurgy, pp. 29–32.

Lopes, J.A., Rosas, C.F., Fernandes, J.B., Vanzela, G.A., 2011. Risk quantification in grade–tonnage curves and resource categorization in a lateritic nickel deposit using geologically constrained joint conditional simulation. Journal of Mining Science 47 (2), 166–176. doi:10.1134/S1062739147020043.

Mariethoz, G., Renard, P., Straubhaar, J., 2010. The direct sampling method to perform multiple-point geostatistical simulations. Water Resources Research 46 (W11536), 1–14. doi:10.1029/2008WR007621.

Mustapha, H., Dimitrakopoulos, R., 2010. High-order stochastic simulation of spatially distributed natural phenomena. Mathematical Geosciences 42 (5). doi:10.1007/s11004-010-9291-8.

Osterholt, V., Dimitrakopoulos, R., 2007. Simulation of wireframes and geometric features with multiple-point techniques: application at Yandi iron ore deposit. 2nd ed. In: Dimitrakopoulos, R. (Ed.), Orebody Modelling and Strategic Mine Planning, Spectrum Series, vol. 14. The Australasian Institute of Mining and Metallurgy, pp. 51–59.

Remy, N., Boucher, A., Wu, J., 2011. Applied Geostatistics with SGeMS: A User's Guide. Cambridge University Press, New York, 284 pp.

Srivastava, R.M., 2005. Probabilistic modeling of ore lens geometry: an alternative to deterministic wireframes. Mathematical Geology 37 (5), 513–544. doi:10.1007/s11004-005-6670-7.

Straubhaar, J., Renard, P., Grégoire, M., Froidevaux, R., Besson, O., 2011. An improved parallel multiple-point algorithm using a list approach. Mathematical Geosciences 43 (3), 305–328. doi:10.1007/s11004-011-9328-7.

Strebelle, S., 2002. Conditional simulation of complex geological structures using multiple-point statistics. Mathematical Geology 34 (1), 1–21. doi:10.1023/A:1014009426274.

Wackernagel, H.J., 2003. Multivariate Geostatistics. Springer-Verlag, Berlin, 256 pp.

Zhang, T., Switzer, P., Journel, A.G., 2006. Filter-based classification of training image patterns for spatial simulation. Mathematical Geosciences 38 (1), 63–80. doi:10.1007/s11004-005-9004-x.